

Faster-Than-Nyquist Equalization with Convolutional Neural Networks

Bruno De Filippo*, Carla Amatetti*, Alessandro Vanelli-Coralli*

*Department of Electrical, Electronic, and Information Engineering (DEI), Univ. of Bologna, Bologna, Italy
{bruno.defilippo, carla.amatetti2, alessandro.vanelli}@unibo.it

Abstract—Faster-than-Nyquist (FTN) signaling aims at improving the spectral efficiency of wireless communication systems by exceeding the boundaries set by the Nyquist-Shannon sampling theorem. 50 years after its first introduction in the scientific literature, wireless communications have significantly changed, but spectral efficiency remains one of the key challenges. To adopt FTN signaling, inter-symbol interference (ISI) patterns need to be equalized at the receiver. Motivated by the pattern recognition capabilities of convolutional neural networks with skip connections, we propose such deep learning architecture for ISI equalization and symbol demodulation in FTN receivers. We investigate the performance of the proposed model considering quadrature phase shift keying modulation and low density parity check coding, and compare it to a set of benchmarks, including frequency-domain equalization, a quadratic-programming-based receiver, and an equalization scheme based on a deep neural network. We show that our receiver outperforms any benchmark, achieving error rates comparable to those in additive white Gaussian noise channel, and higher effective throughput, thanks to the increased spectral efficiency of FTN signaling. With a compression factor of 60% and code rate $3/4$, the proposed model achieves a peak effective throughput of 2.5 Mbps at just 10dB of energy per bit over noise power spectral density ratio, with other receivers being limited by error floors due to the strong inter-symbol interference. To promote reproducibility in deep learning for wireless communications, our code is open source at the repository provided in the references.

Index Terms—Faster-Than-Nyquist Signaling, Inter-Symbol Interference, Deep Learning, Convolutional Neural Networks

I. INTRODUCTION

Since the dawn of wireless communications, one of the greatest challenges has always been how to improve the radio resources utilization. As spectrum is a scarce and costly asset, both academia and industrial researchers have proposed over the years new techniques to increase the number of bits per second that can be transmitted over a fixed bandwidth, *e.g.*, cell-free multiple input multiple output (CF-MIMO) [2] and non-orthogonal multiple access (NOMA) [1]. The appeal of faster-than-Nyquist (FTN) signaling lies in the straightforwardness of its approach: to achieve a higher data rate, one can simply transmit at a faster symbol rate using the same pulse. In 1975, J. E. Mazo investigated the effect of inter-symbol interference (ISI) on symbols transmitted at a rate R_s higher than what the famous Nyquist-Shannon sampling theorem allows, *i.e.*, twice the bandwidth of the modulating pulse. The author observed that, for ideal sinc pulses with bandwidth W and binary transmissions, no significant reduction in minimum euclidean distance between received symbol sequences could

be observed as long as $\frac{2W}{R_s} \geq \tau_{Mazo} = 0.802$, the so-called “Mazo limit” [3]. This result has motivated several authors to investigate FTN and push the technique over the Mazo limit, *e.g.*, [4]–[8]. The scientific community has focused on identifying and exploiting the intricate ISI patterns to equalize the received FTN data streams. Today, after 50 years from Mazo’s original paper, deep learning (DL) techniques are pushing the boundaries of FTN transmissions. In [9], a deep neural network (DNN) was trained to equalize FTN quadrature amplitude modulation (QAM) symbols with a sliding window mechanism. The input of the DNN spans more symbols than those to equalize, leading to a more accurate equalization and, thus, lower block error rate (BLER), at the expense of a slight increase in complexity. To identify the temporal patterns introduced by FTN, recurrent neural networks (RNNs) in FTN were investigated in [10] and [11]. On the one hand, [10] implemented both uni- and bi-directional long-short term memory (LSTM) models to demodulate binary phase shift keying (BPSK) symbols, observing a reduction of the Bit Error Rate (BER) error floor when using the second model over the first. On the other hand, the authors in [11] used a more traditional RNN to equalize FTN BPSK symbols under strong ISI, *i.e.*, with a compression factor $\tau = 0.5$. The DL literature has exponentially grown in the past decade, with image processing and pattern recognition being among the fundamental areas of research. Inspired by the great performance of convolutional neural networks (CNNs) with skip connections in image processing, *e.g.*, [12], we investigate whether such results apply to the physical layer of wireless communication systems, too. CNNs have already been successfully employed in studies related to physical layer techniques, *e.g.*, for NOMA [1] and channel prediction [13]. To the best of our knowledge, their application to FTN has only been proposed for the assistance of the sum-product detection algorithm in [14], where CNNs act as function nodes for the FTN factor graph, approaching the BER analytical bound for convolutionally-coded and BPSK-modulated transmissions. A comprehensive approach to FTN equalization with CNNs, exploiting their pattern recognition capabilities to the fullest, has not been evaluated yet. Motivated by these considerations and analyses, in this paper we:

- Propose the application of CNNs with skip connections in FTN receivers to identify and equalize ISI patterns;
- Evaluate and compare the BER, BLER, and throughput

(TP) achieved by the proposed model against several benchmarks, including a DL-based equalization scheme.

In addition, in an effort to advocate for reproducibility, taking once again inspiration from the DL scientific community, we open-source our code in a public repository [15].

II. SYSTEM MODEL

We here consider a typical transmission and reception chain, consisting of a bit source, a channel encoder, an interleaver, a digital modulator, and pulse shaping on the transmitter side, and a matched filter, a sampler at FTN rate R_s , a demodulator, a deinterleaver, and a channel decoder on the receiver side. The focus of this work is the demodulator, which is here implemented with a CNN. The system employs low density parity check (LDPC) codes. The FTN baseband signal is modeled as follows. A sequence of energy-normalized quadrature phase shift keying (QPSK) symbols $\{x_n\}_{n \in \mathbb{Z}}$ is generated at the output of the digital modulator and fed to the FTN pulse shaper with symbol time $T_s = \frac{1}{R_s} = \tau \frac{1}{2W} = \tau T_N$, where $0 < \tau < 1$ is the FTN compression factor and T_N is the symbol time at Nyquist rate. The filter, employing the unit-energy squared root raised cosine (SRRC) pulse $h(t)$ with roll-off factor $\beta = 0.5$ and bandwidth W , produces the following FTN baseband signal [9]:

$$s(t) = \sum_{n=-\infty}^{+\infty} x_n h(t - n\tau T_N). \quad (1)$$

Clearly, the strict upper constraint on τ results in a violation of the Nyquist-Shannon sampling theorem; thus, as anticipated in the introduction, ISI is introduced in the signal (Figure 1). The waveform is corrupted by additive white Gaussian noise (AWGN), represented by the zero-mean circularly symmetric Gaussian random process $n(t)$ with variance $\frac{N_0}{2}$, with N_0 being the noise power spectral density; then, it is processed by a filter matched to $h(t)$. Calling $g(t) = \int h(\tau)h^*(\tau-t)d\tau$ the ISI channel autocorrelation function, and $\eta(t) = \int n(\tau)h^*(\tau-t)d\tau$ the matched filter response to AWGN [7], the output of the matched filter is:

$$y(t) = \sum_{n=-\infty}^{+\infty} x_n g(t - k\tau T_N) + \eta(t). \quad (2)$$

Sampling at FTN rate R_s results in a sequence $\{y_k\}_{k \in \mathbb{Z}}$, where each received symbol can be computed as

$$y_k = \sum_{n=-\infty}^{+\infty} x_n g((n-k)\tau T_N) + \eta(k\tau T_N), \quad (3)$$

or, considering a block of N_s symbols $\mathbf{y} = \{y_k\}_{1, \dots, N_s}$,

$$\mathbf{y} = \mathbf{G}\mathbf{x} + \boldsymbol{\eta}. \quad (4)$$

In Equation (4), \mathbf{G} represents the ISI channel matrix, *i.e.*, the contribution of previous and successive symbols on the current one due to ISI. We truncate the channel autocorrelation function samples $\{g_n\}_{n \in \mathbb{Z}}$ to the centermost $2L_I + 1 < N_s$ taps, where L_I represents the one-sided ISI span, resulting

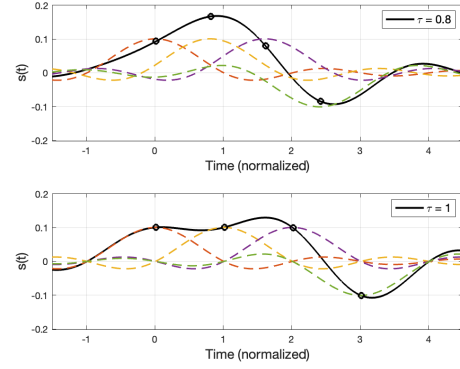


Fig. 1. Example of FTN baseband signal (above) vs at-Nyquist baseband signal (below) corresponding to 4 binary symbols and sinc shaping pulse.

in \mathbf{G} being structured as a $N_s \times N_s$ Toeplitz matrix with $2 \times (N_s - L_I - 1)$ zero diagonals [6]:

$$\mathbf{G} = \begin{bmatrix} 1 & g_{-1} & \cdots & g_{-L_I} & 0 & 0 & \cdots \\ g_1 & 1 & \ddots & \ddots & g_{-L_I} & 0 & \ddots \\ \vdots & \ddots & \ddots & g_{-1} & \ddots & \ddots & \ddots \\ g_{L_I} & \ddots & g_1 & 1 & g_{-1} & \ddots & \ddots \\ 0 & g_{L_I} & \ddots & g_1 & 1 & \ddots & \ddots \\ 0 & 0 & \ddots & \ddots & \ddots & \ddots & \ddots \\ \vdots & \ddots & \ddots & \ddots & \ddots & \ddots & \ddots \end{bmatrix} \quad (5)$$

Note that the structure of \mathbf{G} does not fully reflect the entire ISI at the boundaries, *e.g.*, y_1 is affected only by the upcoming symbols in the block and not by previous transmissions; hence, this effect should be taken into account when simulating a continuous stream of data. The random vector $\boldsymbol{\eta} \sim \mathcal{N}(\mathbf{0}, \frac{N_0}{2} \mathbf{G})$ represents the effect of AWGN after the matched filter, resulting in colored noise. While some works have applied methods to whiten the noise, *e.g.*, [6], we chose to not further manipulate our samples. Thus, \mathbf{y} is the input data of the proposed CNN.

III. PROPOSED CNN-BASED FTN DEMODULATOR

The task of the DL model is to convert a sequence of received symbols into the corresponding sequence of bits. The receiver proposed in this work takes inspiration from pattern recognition models and employs a sequence of 1-dimensional convolutional (Conv1D) layers, leaky rectified linear unit (LReLU) activation functions, and batch normalization (BN) layers, together with skip connections; its structure is reported in detail in Figure 2. Each Conv1D layer acts as a set of $N^{(f)}$ optimized filters with $W^{(f)}$ taps, where each filter is applied to all the D channels of the input tensor to generate a new real-valued sequence of length L ; thus, the number of channels of the output tensor coincides with $N^{(f)}$. Its length depends on the amount P of padding applied before filtering ($P = \text{"same"}$ implies that the sequence length

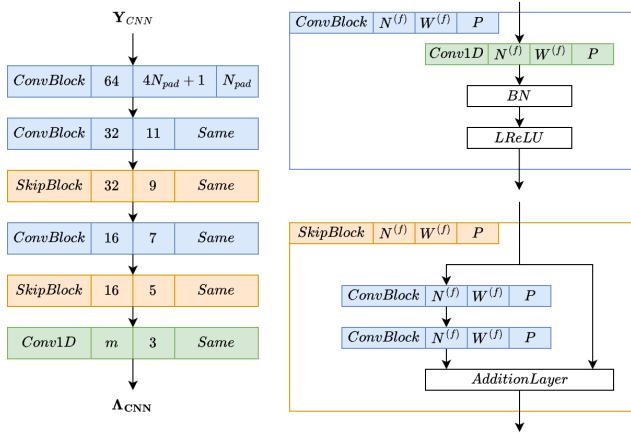


Fig. 2. Diagram of the proposed CNN.

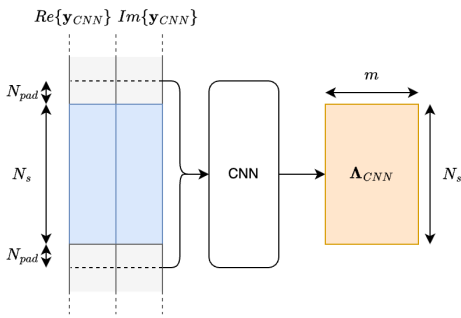


Fig. 3. CNN input pre-processing.

remains unchanged). LReLU activation functions introduce non-linearities in the CNN, allowing both positive and negative activations, differently from their non-leaky counterpart. BN layers normalize a Conv1D layer's activations, resulting in a more stable training process. Finally, skip connections allow Conv1D layers to extract features and apply them to their input tensor, rather than directly outputting the modified input; this enables the effective training of deeper CNNs.

A. CNN input

The pre-processing steps to obtain the CNN input are depicted in Figure 3. A block of N_s received symbols \mathbf{y} is padded on the left with the last N_{pad} symbols of the preceding block and on the right with the first N_{pad} symbols of the upcoming block; we refer to such complex vector of length $L_{in} = N_s + 2N_{pad}$ as \mathbf{y}_{CNN} . While this method delays by $N_{pad}T_s$ the demodulation, it allows the CNN to better extract ISI patterns. The vector is then split into its real and imaginary components, which are stacked together to form a $L_{in} \times 2$ matrix \mathbf{Y}_{CNN} .

B. CNN output

To exploit the capabilities of the LDPC decoder at its full potential, the CNN outputs the bit log likelihood ratios (LLRs) related to the data block of interest. We call such $N_s \times m$ matrix Λ_{CNN} , where the i -th row contains the vector of m LLRs associated to the i -th data symbol in the block. The

corresponding $N_s \times m$ matrix of transmitted bits, to be used as labels during the training process, is referred to as \mathbf{B} .

C. Loss function

While LLRs assume values in \mathbb{R} , it is still possible to approach the problem as a classification task. Conventionally, bit probabilities can be obtained at the output of a DL model by using the binary crossentropy (BCE) loss function if the sigmoid activation function $\sigma(x) = (1 + e^{-x})^{-1}$ is applied to the last layer. Rather than further processing this output, the model can be trained to directly output LLRs by simply moving the sigmoid activation function to the loss function. This results in the so-called BCE with logits (L-BCE) loss function [1], which can be computed by averaging the L-BCE between each LLR $\lambda_i \in \Lambda_{CNN}$ and the corresponding true bit $b_i \in \mathbf{B}$, $L - BCE_i$:

$$L - BCE_i = \begin{cases} \ln(1 + e^{\lambda_i}) & \text{if } b_i = 0 \\ \ln(1 + e^{-\lambda_i}) & \text{if } b_i = 1 \end{cases} \quad (6)$$

D. Dataset, training, and inference

The CNN is pre-trained on a synthetic dataset with no predefined size, *i.e.*, a batch of N_B input matrices and their corresponding labels are generated during each epoch according to the system model presented in Section II. The E_s/N_0 ratio, where $E_s = \mathbb{E}[|x_n|^2]$ is the average energy per symbol, is randomly set for each example within a batch. The gradients of the loss function with respect to the CNN parameters are computed with backpropagation; then, the Adam optimizer updates such parameters using L2 regularization. The learning rate is reduced at loss function plateaus; after long plateaus, early stopping terminates the training process. We separately train one network per value of τ . Once training is completed, the models can be deployed for inference in the receiving chain; online training is out of the scope of this work.

IV. RESULTS

In this section, we analyze the performance of the proposed receiver at the link level. The simulation was carried out in the MATLAB computing environment with the aid of the CVX package [17]; the code is openly available at [15]. Due to space constraints, we report only the main simulation parameters in table I. To ensure that boundary conditions in the ISI channel matrix \mathbf{G} do not affect the validity of our results, we add further padding to each generated block of symbols, simulating a continuous stream; thus, each symbol fed to the CNN is equally affected by ISI.

A. Benchmark receivers

For a complete evaluation, we chose a set of benchmark FTN receivers from the literature to implement alongside our receiver. Here follows a brief description of each of them.

- FTN-agnostic minimum euclidean distance (MED) [16]: the optimal symbol-by-symbol QAM demodulator in AWGN without any FTN-dedicated pre-processing.
- Frequency-domain equalization (FDE) [7]: a cyclic prefix (CP) of length $2\nu_{FDE}$ is added to the symbols block,

TABLE I
SIMULATION PARAMETERS

Parameter	Value
Training E_b/N_0 range	$E_b/N_0 = [-10, 10]$ [dB]
Maximum Monte Carlo Iterations	$N_{MC} = 10^5$
Modulation	QPSK ($m = 2$)
Code rate	$R_c = \{1/2, 3/4\}$
FTN compression	$\tau = \{0.6, 0.7\}$
SRRC roll-off	$\beta = 0.5$
One-sided ISI span	$L_I = \{33, 28\}$ symbols
Nyquist symbol time	$T_N = 1\mu s$
Block size	$N_s = 50$ symbols
Block padding	$N_{pad} = 12$ symbols
Batch size	$N_B = 4096$
Initial learning rate	0.01
Learning rate decay factor	10
Learning rate decay patience	50 epochs
Early stopping patience	150 epochs
L2 regularization factor	10^{-4}

transforming \mathbf{G} in a circulant matrix. The minimum mean squared error (MMSE) detection algorithm is then applied on the Fourier transform of the received symbols.

- Set theory semi-definite-relaxation-based sequence estimation (STSDRSE) [8]: the FTN sequence detection task is modeled as a non-convex optimization problem, of which a relaxed version with quadratic constraint is solved. Gaussian randomization ensures the original constraints are satisfied. To achieve accurate BER plots with reasonable processing time, we limited the number of Monte Carlo iterations with this receiver to 10^4 .
- DNN [9]: a DNN with 4 hidden layers that equalizes the received symbols, resulting in an ideally ISI-free sequence of symbols to be fed to the MED receiver. In a similar fashion to our receiver, a sliding window mechanism extracts a sequence of symbols with padding. We underline the fact that the original paper does not specify all parameters required to ensure full reproducibility. *E.g.*, the input and output length of the DNN are not mentioned in [9]; using a solver, we extrapolated a fair guess for their value based on the reported computational complexity and hidden layers size. More details on such assumptions are reported on our repository.

B. Bit Error Rate

We first assess the uncoded BER as a function of the E_b/N_0 ratio, where $E_b = \frac{E_s}{m}$ is the energy per bit in the FTN signal (Figure 4). The black dashed curve reports the theoretical BER with QPSK in AWGN channel (*i.e.*, with $\tau = 1$). The plot shows that the proposed receiver outperforms all reported benchmarks. At $\tau = 0.7$, the CNN reaches $BER = 10^{-3}$ at 8.5 dB of E_b/N_0 , achieving a gain of 2 dB against the DNN benchmark and being distant 2 dB from ISI-free performance. STSDRSE performs similarly, although requiring much longer to converge on the optimization problem solution. Moving to $\tau = 0.6$, the stronger ISI widens the performance gap, with the CNN reaching a BER of 1.5×10^{-3} at 10 dB of E_b/N_0 ; on the

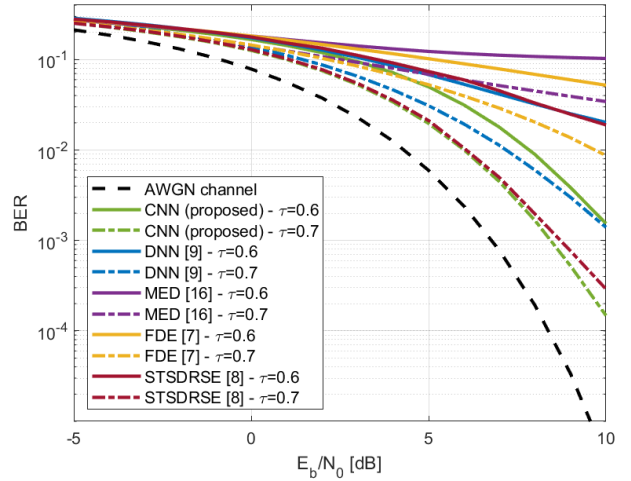


Fig. 4. BER as a function of E_b/N_0 .

opposite, the DNN and STSDRSE benchmarks do not reach the 10^{-2} threshold. Both compression factors introduce too strong ISI for FDE, resulting in unsatisfactory performance. Without any form of equalization, the ISI-agnostic MED receiver reaches a plateau at $BER = 10^{-1}$ for $\tau = 0.6$. It must be noted that the BER curves we obtained for the DNN benchmark do not match those presented in [9]. We believe the discrepancy is due to different truncation of the channel autocorrelation function samples $\{g_n\}_{n \in \mathbb{Z}}$, leading to different ISI spans L_I , and our consideration of the boundary conditions in \mathbf{G} , which may not have been accounted for in the original work. Nonetheless, our open repository includes the code we used to train the DNN benchmark.

C. Block Error Rate

We shift the attention to the analysis of the BLER, reported in Figures 5 and 6 for code rates 3/4 and 1/2, respectively. We obtain a theoretical BLER curve by randomly introducing independent bit errors with probability in accordance to the theoretical BER with AWGN channel. At the least strong compression factor, the LDPC decoder corrects most of the errors that the CNN was not able to mitigate, leading to a BLER close to ISI-free error rates; the performance at $\tau = 0.6$ does not worsen by much, with $BER = 10^{-3}$ being achieved at 6.5 dB of E_b/N_0 (3dB from AWGN). On the opposite, the DNN requires almost 4dB more of E_b/N_0 to reach the same threshold, *i.e.*, it achieves a 0.1% BLER at an E_b/N_0 level higher than 10dB. When the code rate is increased to 3/4, the ISI equalization capabilities of the DNN are not adequate for a perfect demodulation, and an error floor is revealed over $BER = 10^{-2}$. As in the BER plots, FDE and MED are the least performing receivers, with MED not even reaching a 10% of BLER. As previously mentioned, we do not include STSDRSE plots here due to the excessive simulation time required to achieve accurate results at high E_b/N_0 ; nonetheless, we note that the algorithm tended to be outperformed by the DNN benchmark for both values of τ .

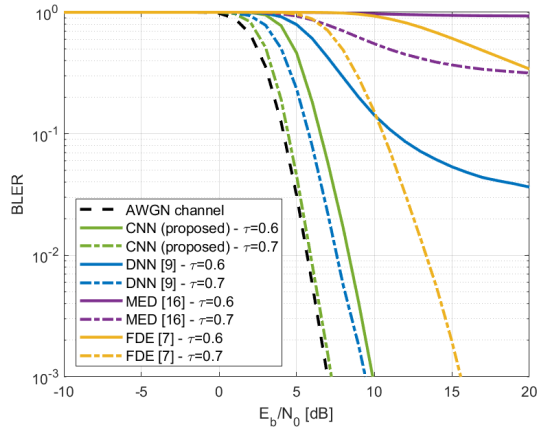


Fig. 5. BLER as a function of E_b/N_0 for code rate $R_c = 3/4$.

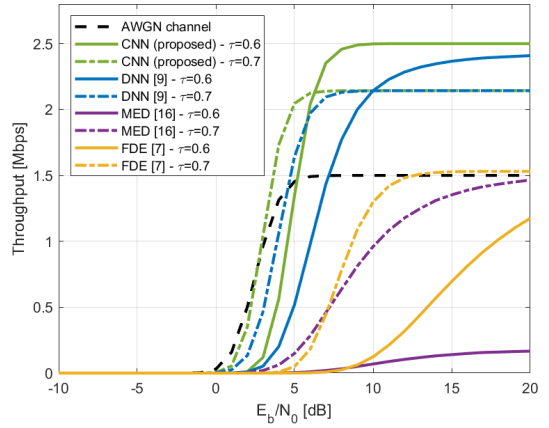


Fig. 7. Throughput as a function of E_b/N_0 for code rate $R_c = 3/4$.

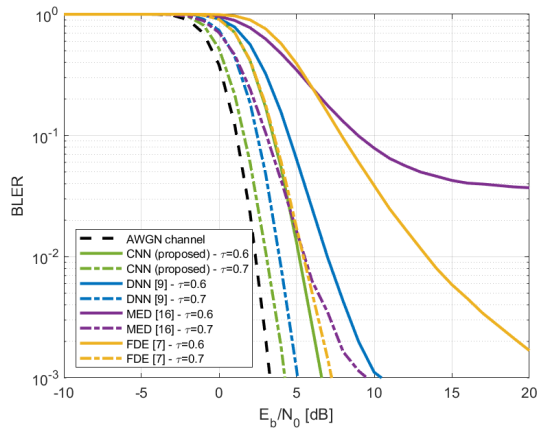


Fig. 6. BLER as a function of E_b/N_0 for code rate $R_c = 1/2$.

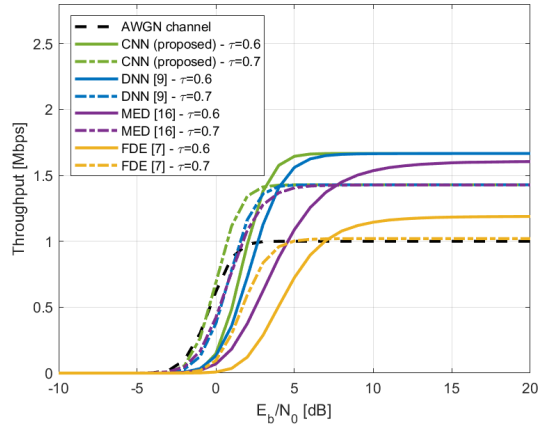


Fig. 8. Throughput as a function of E_b/N_0 for code rate $R_c = 1/2$.

D. Throughput

The attractiveness of FTN lies in the potential achieved TP; however, the metric does not only depend on the symbol rate at the transmitter, but also on the capabilities of the receiver:

$$TP = \frac{m \cdot R_c}{\tau \cdot T_N} \cdot \gamma \cdot (1 - BLER), \quad (7)$$

where $\gamma = \frac{N_s}{N_s + 2V_{FDE}}$ in FDE, to account for the addition of the CP, and $\gamma = 1$ for other receivers. Clearly, the AWGN channel TP employs $\tau = 1$. We investigate the TP gains achieved by the CNN with respect to transmissions at Nyquist rate, comparing such results with the considered FTN benchmarks. Regardless of the code rate, Figures 7 and 8 reveal that FTN is not beneficial to the TP at low E_b/N_0 ; this is due to the increased error rate in blocks transmitted at FTN rate. However, the introduction of the CNN manages to overcome the AWGN TP with lower E_b/N_0 than any other FTN receiver (2.5dB and -0.5dB for code rate 3/4 and 1/2, respectively). At $R_c = 1/2$, the proposed receiver reaches its peak TP of 1.47 Mbps and 2.14 Mbps ($\tau = 0.6$ and 0.7, respectively) with a gain of 1-2 dB of E_b/N_0 with respect to the DNN benchmark; however, the DNN fails at reaching its peak throughput with high code rate and strong

FTN compression due to the BLER error floor, while the CNN easily achieves 2.5 Mbps at 10dB of E_b/N_0 . It must be noted that the highest obtainable TP curve is achieved by the proposed receiver after $E_b/N_0 = -0.5$ dB setting $\tau = 0.7$, then decreasing the coding rate at 3.5dB, and finally switching to $\tau = 0.6$ at 6dB. Indeed, the compression factor can be added as a third dimension to adaptive code and modulation, leading to better TP at any E_b/N_0 working point if a powerful FTN receiver, such as the proposed CNN, is implemented.

V. COMPUTATIONAL COMPLEXITY

We showed that CNNs can provide substantial throughput gains in FTN. However, computational complexity is also a key parameter to take into consideration. We evaluate the number of multiply-and-accumulate (MAC) units in a Conv1D layer as $M_{Conv1D} = LDW^{(f)}N^{(f)}$; the additional complexity of BN and LReLU is negligible. Considering the model reported in Figure 2, the total amount of MAC operations amounts to 2.67M, or 53.5k MACs per received symbol. On the opposite, the DNN benchmark only requires 8196 multiplications per symbol [9], limiting the number of required MAC units per symbol to such value. Despite the increase in MACs, three key considerations should be taken into account.

I) Given the vast amount of tunable parameters in CNNs, it is possible that specific parameter combinations providing comparable link-level performance with lower computational complexity were missed. II) Model compression techniques, which are out of the scope of this work, can greatly reduce the number of MAC units required by the proposed FTN receiver with negligible performance losses or, in some cases, even marginal gains [18]. III) Specialized hardware accelerators can allow running inference with large DL models with small processing time; even with stringent power and size constraint, *e.g.*, on board of small unmanned aerial vehicles, a CNN with 1.1M MACs can run at 139 inferences/s [19]. Hence, the adoption of model compression techniques and hardware accelerators make the CNN-based FTN receivers a feasible solution from the computational complexity standpoint.

VI. CONCLUSIONS

In this work, motivated by recent advances of DL in pattern recognition tasks, we proposed the application of CNNs to FTN receivers. We trained a CNN with skip connections and evaluated its performance in terms of BER, BLER, and TP against several benchmarks. In an effort to advocate for reproducibility, we open-sourced our code in a public repository. The proposed model achieves BLER levels at less than 1dB and 3.5dB of E_b/N_0 from AWGN channel performance for $\tau = 0.7$ and $\tau = 0.6$, respectively, outperforming all reported benchmarks. Such gains are reflected in the TP, as the low BLER achieved by the CNN enables the spectral efficiency benefits of FTN to be fully exploited. Indeed, with $\tau = 0.6$ the TP reaches 2.5 Mbps at $E_b/N_0 = 10$ dB, while the DNN-based benchmark is limited by the strong ISI. 50 years after the publication of Mazo's original paper, thanks to CNNs, we proved that FTN has more potential than ever. As current cellular systems employ multi-carrier transmissions, FTN transceivers have recently been proposed for orthogonal frequency division multiplexing (OFDM), *e.g.*, [20]. With the possible introduction of inter-carrier interference in addition to ISI, we aim at extending the CNN presented in this work to a 2-dimensional case for FTN OFDM receivers and to more complex channel models.

VII. ACKNOWLEDGMENTS

This work was partially supported by the European Union under the Italian National Recovery and Resilience Plan (NRRP) of NextGenerationEU, partnership of "Telecommunications of the Future" (PE00000001 - program "RESTART"), and by the 6G-NTN project, which received funding from the Smart Networks and Services Joint Undertaking (SNS JU) under the European Union's Horizon Europe research and innovation programme under Grant Agreement No 101096479. The views expressed are those of the authors and do not necessarily represent the project. The Commission is not liable for any use that may be made of any of the information contained therein.

REFERENCES

- [1] B. De Filippo et al., "An SCMA Receiver for 6G NTN based on Multi-Task Learning," Accepted for 2024 IEEE Global Communications Conference Workshops (GC Wkshps), Cape Town, South Africa, December 2024.
- [2] A. Guidotti, A. Vanelli-Coralli and C. Amatetti, "Federated Cell-Free MIMO in Nonterrestrial Networks: Architectures and Performance," in IEEE Transactions on Aerospace and Electronic Systems, vol. 60, no. 3, pp. 3319-3347, June 2024, doi: 10.1109/TAES.2024.3362769.
- [3] J. E. Mazo, "Faster-than-nyquist signaling," in The Bell System Technical Journal, vol. 54, no. 8, pp. 1451-1462, Oct. 1975, doi: 10.1002/j.1538-7305.1975.tb02043.x.
- [4] J. B. Anderson, A. Prlja and F. Rusek, "New reduced state space BCJR algorithms for the ISI channel," 2009 IEEE International Symposium on Information Theory, Seoul, Korea (South), 2009, pp. 889-893, doi: 10.1109/ISIT.2009.5205622.
- [5] A. Prlja and J. B. Anderson, "Reduced-Complexity Receivers for Strongly Narrowband Intersymbol Interference Introduced by Faster-than-Nyquist Signaling," in IEEE Transactions on Communications, vol. 60, no. 9, pp. 2591-2601, September 2012, doi: 10.1109/TCOMM.2012.070912.110296.
- [6] S. Li et al., "Reduced-Complexity Equalization for Faster-Than-Nyquist Signaling: New Methods Based on Ungerboeck Observation Model," in IEEE Transactions on Communications, vol. 66, no. 3, pp. 1190-1204, March 2018, doi: 10.1109/TCOMM.2017.2774816.
- [7] S. Sugiura, "Frequency-Domain Equalization of Faster-than-Nyquist Signaling," in IEEE Wireless Communications Letters, vol. 2, no. 5, pp. 555-558, October 2013, doi: 10.1109/WCL.2013.072313.130408.
- [8] E. Bedeer, M. H. Ahmed and H. Yanikomeroğlu, "Low-Complexity Detection of High-Order QAM Faster-Than-Nyquist Signaling," in IEEE Access, vol. 5, pp. 14579-14588, 2017, doi: 10.1109/ACCESS.2017.2719628.
- [9] P. Song, F. Gong, Q. Li, G. Li and H. Ding, "Receiver Design for Faster-Than-Nyquist Signaling: Deep-Learning-Based Architectures," in IEEE Access, vol. 8, pp. 68866-68873, 2020, doi: 10.1109/ACCESS.2020.2986679.
- [10] S. Lai and M. Li, "Recurrent Neural Network Assisted Equalization for FTN Signaling," ICC 2020 - 2020 IEEE International Conference on Communications (ICC), Dublin, Ireland, 2020, pp. 1-6, doi: 10.1109/ICC40277.2020.9148769.
- [11] S. Paul, N. Seshadri and R. D. Koilpillai, "Deep-Learning based Equalization of Highly Compressed Faster Than Nyquist Signals," 2023 IEEE International Conference on Advanced Networks and Telecommunications Systems (ANTS), Jaipur, India, 2023, pp. 396-401, doi: 10.1109/ANTS59832.2023.10469596.
- [12] W. Quan et al., "Image Inpainting With Local and Global Refinement," in IEEE Transactions on Image Processing, vol. 31, pp. 2405-2420, 2022, doi: 10.1109/TIP.2022.3152624.
- [13] J. Yuan, H. Q. Ngo and M. Matthaiou, "Machine Learning-Based Channel Prediction in Massive MIMO With Channel Aging," in IEEE Transactions on Wireless Communications, vol. 19, no. 5, pp. 2960-2973, May 2020, doi: 10.1109/TWC.2020.2969627.
- [14] B. Liu, S. Li, Y. Xie and J. Yuan, "A Novel Sum-Product Detection Algorithm for Faster-Than-Nyquist Signaling: A Deep Learning Approach," in IEEE Transactions on Communications, vol. 69, no. 9, pp. 5975-5987, Sept. 2021, doi: 10.1109/TCOMM.2021.3090026.
- [15] B. De Filippo, C. Amatetti, and A. Vanelli-Coralli. "DeepFTN", v1.0. November 2024 [Online]. Available: <https://github.com/Defil1998/DeepFTN>
- [16] S. Benedetto and E. Biglieri, "Principles of digital transmission: with wireless applications", Springer Science & Business Media, 2005.
- [17] CVX Research, Inc. "CVX: Matlab software for disciplined convex programming", v2.0. April 2011 [Online]. Available:<https://cvxr.com/cvx>
- [18] J. Guo et al., "Compression and Acceleration of Neural Networks for Communications," in IEEE Wireless Communications, vol. 27, no. 4, pp. 110-117, August 2020, doi: 10.1109/MWC.001.1900473.
- [19] L. Lamberti et al., "Distilling Tiny and Ultra-fast Deep Neural Networks for Autonomous Navigation on Nano-UAVs," in IEEE Internet of Things Journal (in press), doi: 10.1109/IIOT.2024.3431913.
- [20] K. Wang, A. Liu, X. Liang, S. Peng and Q. Zhang, "A Faster-Than-Nyquist (FTN)-Based Multicarrier System," in IEEE Transactions on Vehicular Technology, vol. 68, no. 1, pp. 947-951, Jan. 2019, doi: 10.1109/TVT.2018.2861823.